Since January 2020 Elsevier has created a COVID-19 resource centre with free information in English and Mandarin on the novel coronavirus COVID-19. The COVID-19 resource centre is hosted on Elsevier Connect, the company's public news and information website.

Bioorganic & Medicinal Chemistry Letters 27 (2017) 3019–3025

Contents lists available at ScienceDirect

Bioorganic & Medicinal Chemistry Letters

journal homepage: www.elsevier.com/locate/bmcl

Antiviral escin derivatives from the seeds of *Aesculus turbinata* Blume (Japanese horse chestnut)

Ji Won Kim [a,e], Thi-Kim-Quy Ha [a,e], Hyomoon Cho [a], Eunhee Kim [b], Sang Hee Shim [c], Jun-Li Yang [d], Won Keun Oh [a,*]

[a] Korea Bioactive Natural Material Bank, Research Institute of Pharmaceutical Sciences, College of Pharmacy, Seoul National University, Seoul 151-742, Republic of Korea
[b] Choong Ang Vaccine Laboratory, 59-3 Hwaam-dong, Yuseong-gu, Daejeon 305-348, Republic of Korea
[c] College of Pharmacy, Duksung Women's University, Seoul, Republic of Korea
[d] Key Laboratory of Chemistry of Northwestern Plant Resources of CAS and Key Laboratory for Natural Medicine of Gansu Province, Lanzhou Institute of Chemical Physics, Chinese Academy of Sciences, Lanzhou 730000, PR China

ARTICLE INFO

Article history:
Received 8 April 2017
Revised 4 May 2017
Accepted 6 May 2017
Available online 8 May 2017

Keywords:
Porcine epidemic diarrhea virus (PEDV)
Horse chestnut
Aesculus turbinata
Escins

ABSTRACT

Porcine epidemic diarrhea virus (PEDV) causes severe diarrhea and high fatality of piglets, influencing the swine industry. Japanese horse chestnut (seed of *Aesculus turbinata*) contains many saponin mixtures, called escins, and has been used for a long time as a traditional medicinal plant. Structure-activity relationship (SAR) studies on escins have revealed that acylations at C-21 and C-22 with angeloyl or tigloyl groups were important for their cytotoxic effects. However, the strong cytotoxicity of escins makes them hard to utilize for other diseases and to develop as nutraceuticals. In this research, we investigated whether escin derivatives **1**–**7** (including new compounds **2**, **3**, **5** and **6**), without the angeloyl or tigloyl groups and with modified glycosidic linkages by hydrolysis, have PEDV inhibitory effects with less cytotoxicity. Compounds **1**–**7** had no cytotoxicity at 20 μM on VERO cells, while compounds **8**–**10** showed strong cytotoxicity at similar concentrations on PEDV. Our results suggest that escin derivatives showed strong inhibitory activities on PEDV replication with lowered cytotoxicity. These studies propose a method to utilize Japanese horse chestnut for treating PEDV and to increase the diversity of its bioactive compounds.

Coronaviruses (CoVs) have been reported as the causes of different diseases at respiratory, enteric or central nervous system in many species including bats, pigs, horses and humans.[1] These viruses are enveloped and single-stranded RNA viruses, constituting the largest RNA genomes in mammalian viruses, ranging from 25.5 to nearly 32 kb in length.[2] Until 2003, only two coronaviruses were identified as infecting humans. However, severe acute respiratory syndrome coronavirus (SARS-CoV), was newly identified in 2002 to 2003, causing 10–50% mortality in infected individuals, affecting 27 countries, and exhibiting atypical pneumonia.[1,2] A novel coronavirus, Middle East respiratory syndrome coronavirus (MERS-CoV), was first isolated and reported in Saudi Arabia in 2012. The symptoms of MERS-CoV include acute pneumonia and severe renal failure in humans after infection.[3] This disease continued to emerge and spread to approximately 30 countries[4] and in May 2015, an outbreak of MERS occurred in the Korea via a traveler from the Middle East. Until the patient was diagnosed as infected with MERS-CoV, 29 secondary infections occurred by visiting different clinics, resulting in 186 confirmed cases.[5]

Coronaviruses at a molecular level have important features such as high rates of RNA recombination, extraordinarily large RNA genomes and rapid stability after transmission to other species, and leading to genetic diversity, unlike other enveloped RNA viruses.[6] PEDV of family *Coronaviridae* shares phylogenetically common features with other coronaviruses. PEDV causes severe diarrhea, dehydration, vomiting in pigs of all ages, and high mortality of piglets, resulting in tremendous financial loss.[7] Thus, these results imply the necessity of studying the characteristics of coronaviruses and discovering active drugs to prevent the fast and extensive spread of coronaviruses.

Aesculus L (Hippocastanaceae) contains 12 species of deciduous trees and has been cultivated as pharmaceutical crops for the production of Standardized Therapeutics Extracts of escins in China. The common name "horse chestnut" came from the uses of seeds for horses to treat overexertion or coughs, and it has been used as therapeutics purposes for anti-fever.[8] Japanese horse chestnut

* Corresponding author.
E-mail address: wkoh1@snu.ac.kr (W.K. Oh).
[e] These authors contributed equally to this work.

http://dx.doi.org/10.1016/j.bmcl.2017.05.022
0960-894X/

(*Aesculus turbinata*) is a medicinal plant widely distributed in Japan and also has a small amount of cultivation in Korea and China.[9] The seeds, which a large amount of escins were reported as its constituents,[9] have been used for diverse biological activities including anti-inflammatory, anti-obesity, hypoglycemic, and anti-cancer effects.[10–14]

Escins were also reported to possess strong antiviral effects against SARS-CoV with an EC_{50} of 6.0 μM (SI value of 2.5)[15] and against anti-HIV-1 protease.[9] However, the industrial utilization of escins for application to diseases and development as nutraceuticals has been limited to date due to their strong nonspecific cytotoxic effects. These reports prompted us towards the development of safer escin derivatives with anti-CoV activities. Previous studies on structure–activity relationship with escins suggested that acylation at C-21 and C-22 was necessary for the cytotoxic effects.[16–20] The cytotoxicity can be enhanced with methylation at C-24 and a free hydroxyl at C-16 at oleanane-type structure and altered by the site of glycosides.[14,21] Thus, alkaline and acid hydrolysis of escins was applied to detach acyl moieties at C-21 and C-22, and provide varieties of sugar moieties at C-3.

In this research, we reported ten compounds (**1**–**10**), including four new compounds **2**, **3**, **5** and **6**, from the extract of *A. turbinate* after the two-step hydrolysis. We also measured their antiviral activities using the PEDV assay with isolated compounds and each fraction for safer utilization of Japanese horse chestnut.

The air-dried seeds of *A. turbinata* were extracted and separated through column chromatography using silica gel, RP-C_{18} and preparative HPLC to afford ten compounds, including four new (**2**, **3** and **5, 6**) and six known (**1**, **4** and **7**–**10**).[22,23]

Compound **2** was obtained as a brownish amorphous powder. The positive HRESIMS showed $[(M+H)+[-H_2O]]^+$ ion at *m*/*z* 649.3946 (calcd for 649.3946) and $[M-H]^-$ ion at *m*/*z* 665.3901 (calcd for 665.3906), implying the molecular formula to be $C_{36}H_{58}O_{11}$. The IR spectrum showed absorption due to hydroxyl

Table 1
^{1}H NMR and ^{13}C NMR spectroscopic data of compounds **2**, **3**, **5**, and **6** in pyridine-d_5.

No.	**2**[a]		**3**[a]		**5**[b]		**6**[b]	
	δ_C	δ_H (*J* in Hz)	δ_C	δ_H (*J* in Hz)	δ_C	δ_H (*J* in Hz)	δ_C	δ_H (*J* in Hz)
1	39.0	1.47, 0.94	39.0	1.45, 0.90	38.9	1.46, 0.91	38.9	1.43, 0.85
2	26.8	1.92, 1.76	26.8	2.24 (d-like; 11.1), 1.85	27.2	2.23 (d-like; 10.2), 2.03 (d-like)	27.1	2.17 (d-like; 12.9), 2.00 (dd-like; 11.0)
3	89.1	3.42 (dd-like)	89.2	3.41 (dd-like)	89.2	3.63 (dd-like; 11.8)	89.3	3.56 (d; 10.8)
4	39.7		39.7		44.7		44.7	
5	56.0	0.80	55.9	0.82	56.4	0.94 (d; 11.5)	56.4	0.91 (d; 12.3)
6	18.6	1.61, 1.50	18.6	1.65, 1.51	19.1	1.65, 1.36	19.1	1.62, 1.35
7	33.4	1.62, 1.32	33.3	1.63, 1.31 (overlap)	33.7	1.59, 1.31	33.7	1.59, 1.30
8	40.2		40.2		40.3		40.3	
9	47.2	1.77	47.2	1.77	47.2	1.76	47.2	1.74 (m)
10	37.0		37.0		36.8		36.8	
11	24.0	1.92, 1.79	24.0	1.93, 1.87	24.4	1.91, 1.80	24.4	1.91, 1.79
12	123.2	5.39 (br s)	123.1	5.42 (br s)	123.2	5.38 (br s)	123.3	5.39 (br s)
13	144.1		144.1		144.2		144.3	
14	42.2		42.2		42.3		42.4	
15	34.5	2.10 (d; 12.3), 1.69 (d; 14.3)	34.5	2.12 (d; 11.8), 1.71 (d; 14.2)	34.6	2.08 (dd-like; 14.5, 3.5), 1.69 (d; 13.5)	34.6	2.08 (d-like; 11.2), 1.68 (d; 13.8)
16	68.0	5.03 (overlap)	68.0	5.04 (overlap)	68.2	5.02 (br s)	68.2	5.02 (br s)
17	47.5		47.5		47.7		47.7	
18	41.3	2.80 (dd-like; 13.0)	41.3	2.82 (dd-like)	41.3	2.80 (dd; 14.0, 3.7)	41.5	2.81 (dd; 13.3, 3.7)
19	48.4	3.06 (t; 13.4), 1.43	48.4	3.08 (t; 13.5)	48.5	3.02 (t; 13.5), 1.42 (dd; 12.9, 4.2)	48.5	3.05 (t; 13.4), 1.42 (d-like)
20	36.6		36.6		36.7		36.8	
21	78.9	4.80 (d; 8.6)	78.8	4.82 (d; 9.5)	79.0	4.80 (d; 9.6)	79.0	4.81 (d; 9.4)
22	77.5	4.63 (d-like; overlap)	77.4	4.65 (d; 9.6)	77.5	4.64 (d; 9.5)	77.5	4.64 (d; 9.5)
23	28.3	1.30	28.3	1.31	23.6	1.53	23.6	1.49
24	17.2	1.00	17.1	1.02	63.6	4.40 (d; 11.2), 3.65 (d; 11.4)	63.5	4.37 (d; 11.0), 3.62 (d; 10.6)
25	16.0	0.85	15.9	0.87	15.8	0.80	15.8	0.78
26	17.1	0.90	17.1	0.92	17.1	0.88	17.2	0.88
27	27.6	1.88	27.6	1.90	27.7	1.88	27.7	1.89
28	68.6	4.02 (d; 10.3), 3.72 (dd; 10.1)	68.5	4.04 (d; 10.6), 3.74 (overlap)	68.5	4.00 (d; 10.5), 3.71 (d; 10.3)	68.6	4.10 (d; 10.3), 3.72 (d; 10.4)
29	30.8	1.32	30.7	1,35	30.9	1.33	30.9	1.33
30	19.6	1.38	19.6	1.43	19.8	1.40	19.8	1.39
GlcA								
1′	107.4	5.03 (overlap)	107.0	5.03 (overlap)	106.7	5.18 (d; 7.4)	106.2	5.09 (overlap)
2′	75.7	4.13 (*t*-like)	75.1	4.15 (*t*-like)	75.7	4.12 (t; 8.2)	75.2	4.11 (overlap)
3′	78.4	4.32 (*t*-like)	76.1	4.37 (t; 7.5)	78.4	4.35 (t; 8.8)	76.9	4.32 (t; 7.2)
4′	73.7	4.58 (overlap)	82.9	4.61 (overlap)	73.9	4.60 (*t*-like)	83.9	4.54 (overlap)
5′	77.9	4.67 (overlap)	76.6	4.75 (d; 7.8)	78.3	4.73 (d-like)	76.9	4.69
6′	n.d		n.d		173.4		n.d	
Glc								
1″			105.0	5.25 (d; 6.4)			105.3	5.22 (overlap)
2″			75.0	4.09 (t; 8.0)			75.4	4.07 (t; 7.3)
3″			78.2	4.23 (overlap)			78.4	4.25 (overlap)
4″			71.7	4.15 (overlap)			72.0	4.12 (overlap)
5″			78.6	4.02 (overlap)			78.8	4.00 (overlap)
6″			62.7	4.53 (d; 11.0), 4.27 (overlap)			62.9	4.52, 4.23 (both overlap)

ppm, *J* in Hz.
[a] Recorded in ^{1}H (500 MHz) and ^{13}C NMR (125 MHz).
[b] Recorded in ^{1}H NMR (800 MHz) and ^{13}C NMR (200 MHz).

(3375 cm^{-1}), olefinic bond (1658 cm^{-1}), and glycosidic linkage (1023 cm^{-1}). The ^{1}H and ^{13}C NMR data of **2** proposed the structure as an olean-12-ene triterpenoid glucopyranosiduronic acid, exhibiting signals for seven tertiary methyl groups [δ_H 0.85 (CH_3-25), 0.90 (CH_3-26), 1.00 (CH_3-24), 1.30 (CH_3-23), 1.32 (CH_3-29), 1.38 (CH_3-30) and 1.88 (CH_3-27)], an olefinic proton at δ_H 5.39 (br s) with two olefinic carbon signals at δ_C 123.0 (C-12) and 144.0 (C-13), and one β-D-glucopyranosiduronic acid moiety [one anomeric proton at δ_H 5.03 (H-1′), along with five carbon signals at δ_C 107.2 (C-1′), 78.2 (C-3′), 77.7 (C-5′), 75.5 (C-2′) and 73.5 (C-4′)] (Table 1). The ^{1}H and ^{13}C NMR data of **2** were consistent with those of escinidin (**1**), except for the chemical shift of C-3 and the presence of one β-D-glucopyranosiduronic acid moiety in **2** (Fig. 1). These results indicated the attachment of β-D-glucopyranosiduronic acid to C-3 (δ_C 89.0). The linkage position of this β-D-glucopyranosiduronic acid was confirmed by the HMBC experiment from the correlation from H-1′ (δ_H 5.03) to C-3 (δ_C 89.1) (Fig. 2A). Therefore, the structure of **2** was elucidated as (3β,16α,21β,22α)-16,21,22,28-tetrahydroxyolean-12-en-3-*O*-β-D-glucopyranosiduronic acid.[23]

Compound **3** was isolated as a brownish amorphous powder, with the molecular formula $C_{42}H_{68}O_{16}$, as implied from the HRESIMS at *m*/*z* 851.4408 $[M+Na]^+$ (calcd for $C_{42}H_{68}O_{16}Na^+$, 851.4400) and at *m*/*z* 827.4434 $[M-H]^-$ (calcd for $C_{42}H_{67}O_{16}^-$, 827.4435). The IR spectrum suggested the presence of hydroxyl (3390 cm^{-1}), olefinic bond (1658 cm^{-1}), and glycosidic linkage (1028 cm^{-1}). The ^{1}H NMR spectrum showed signals for seven tertiary methyl groups [δ_H 0.87 (CH_3-25), 0.92 (CH_3-26), 1.02 (CH_3-24), 1.31 (CH_3-23), 1.35 (CH_3-29), 1.43 (CH_3-30) and 1.90 (CH_3-27)], an olefinic proton at δ_H 5.42 (br s) and two anomeric protons at δ_H 5.25 (1H, d, *J* = 6.4 Hz, H-1″) and 5.03 (1H, d-like, overlap, H-1′). The ^{13}C NMR spectrum of **3** was very similar to that of **2**, apart from the presence of one β-D-glycopyranosyl moiety in **3** (Table 1). The linkage position of the β-D-glycopyranosyl was identified by HMBC experiment. The HMBC correlations between H-3 (δ_H 3.41) and C-1′ (δ_C 107.0) and also H-4′ (δ_H 4.61) and C-1″ (δ_C 105.0) were observed, indicating that β-D-glucopyranosiduronic acid was attached to the carbon C-3 as in **2**, and the other β-D-glycopyranosyl was linked at the C-4′ of β-D-glucopyranosiduronic acid (Fig. 2A). Thus, the structure of **3** was established as (3β,16α,21β,22α)-16,21,22,28-tetrahydroxyolean-12-en-3-yl-*O*-[β-D-glycopyranosyl-(1→4)]-β-D-glucopyranosiduronic acid).[23]

Compound **5** was obtained as a brown amorphous powder. HRESIMS of positive mode showed a $[(M+H)+[-H_2O]]^+$ ion at *m*/*z* 665.3898 (calcd for 665.3895) and $[M-H]^-$ ion at *m*/*z* 681.3852 (calcd for 681.3856), which indicated a molecular formula of $C_{36}H_{58}O_{12}$. Absorption bands at 3385, 1657, and 1028 cm^{-1} in the IR spectrum demonstrated the presence of hydroxyl, olefinic bond, and glycosidic linkage, respectively. The ^{1}H and ^{13}C NMR data of **5** indicated the structure as an olean-12-ene triterpenoid glucopyranosiduronic acid, disclosing the presence of six tertiary methyl groups [δ_H 0.80 (CH_3-25), 0.88 (CH_3-26), 1.33 (CH_3-29), 1.40 (CH_3-30), 1.53 (CH_3-23), 1.88 (CH_3-27)], as well as an olefinic proton at δ_H 5.38 (br s, H-12) with two olefinic carbon signals at δ_C 123.2 (C-12) and 144.2 (C-13), and one β-D-glucopyranosiduronic acid moiety [one anomeric proton δ_H 5.18 (d, *J* = 7.2 Hz, H-1′), along with six carbon signals at δ_C 173.4 (C-6′), 106.7 (C-1′), 78.4 (C-3′), 78.3 (C-5′), 75.7 (C-2′), and 73.9 (C-4′)]. Compound **5** was similar to **2** except for the presence of a hydroxyl group at C-24 (δ_C 63.6) (Table 1). The HMBC correlation between H-3 (δ_H 3.63) and C-1′ (δ_C 106.7) confirmed the position of β-D-glucopyranosiduronic acid. The relative configuration of **5** was investigated by analysis of its ROESY spectrum (Fig. 2B).

Correlations between H_2-24 (δ_H 4.40)/H_3-25 (δ_H 0.80), H_3-25 (δ_H 0.80)/H_3-26 (δ_H 0.88), H_3-26 (δ_H 0.88)/H_2-28 (δ_H 4.00), H_2-28 (δ_H 4.00)/H-16 (δ_H 5.02), H-16 (δ_H 5.02)/H-22 (δ_H 4.64), H-22 (δ_H 4.64)/H_3-30 (δ_H 1.40), H_3-30 (δ_H 1.40)/H-18 (δ_H 2.80), and H-18 (δ_H 2.80)/H-22 (δ_H 4.64) were observed in the ROESY data, implying that all these protons were on the same side of the molecule. The relative configuration of compound **5** remained unaltered even

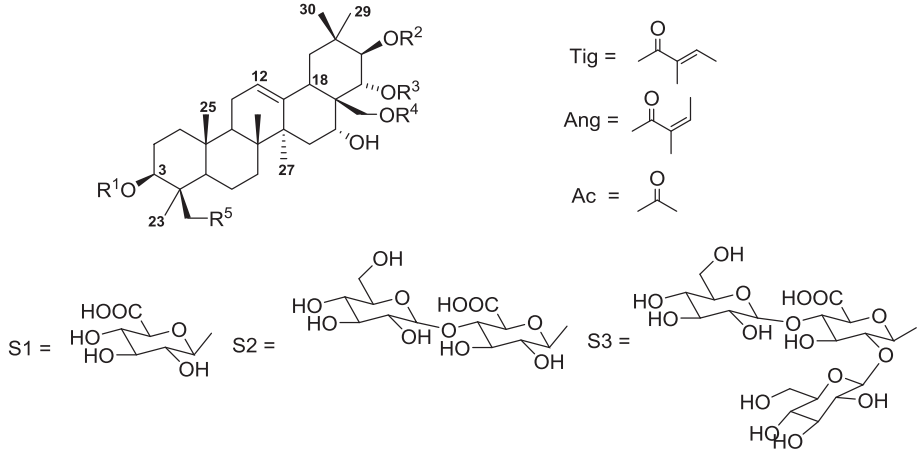

1	R^1 = H	R^2 = H	R^3 = H	R^4 = H	R^5 = H
2	R^1 = S1	R^2 = H	R^3 = H	R^4 = H	R^5 = H
3	R^1 = S2	R^2 = H	R^3 = H	R^4 = H	R^5 = H
4	R^1 = H	R^2 = H	R^3 = H	R^4 = H	R^5 = OH
5	R^1 = S1	R^2 = H	R^3 = H	R^4 = H	R^5 = OH
6	R^1 = S2	R^2 = H	R^3 = H	R^4 = H	R^5 = OH
7	R^1 = S3	R^2 = H	R^3 = H	R^4 = H	R^5 = OH
8	R^1 = S3	R^2 = Tig	R^3 = Ac	R^4 = H	R^5 = OH
9	R^1 = S3	R^2 = Tig	R^3 = H	R^4 = Ac	R^5 = OH
10	R^1 = S3	R^2 = Ang	R^3 = Ac	R^4 = H	R^5 = OH

Fig. 1. Chemical structures of isolated compounds **1**–**10** from *Aesculus turbinata* and its reaction mixture.

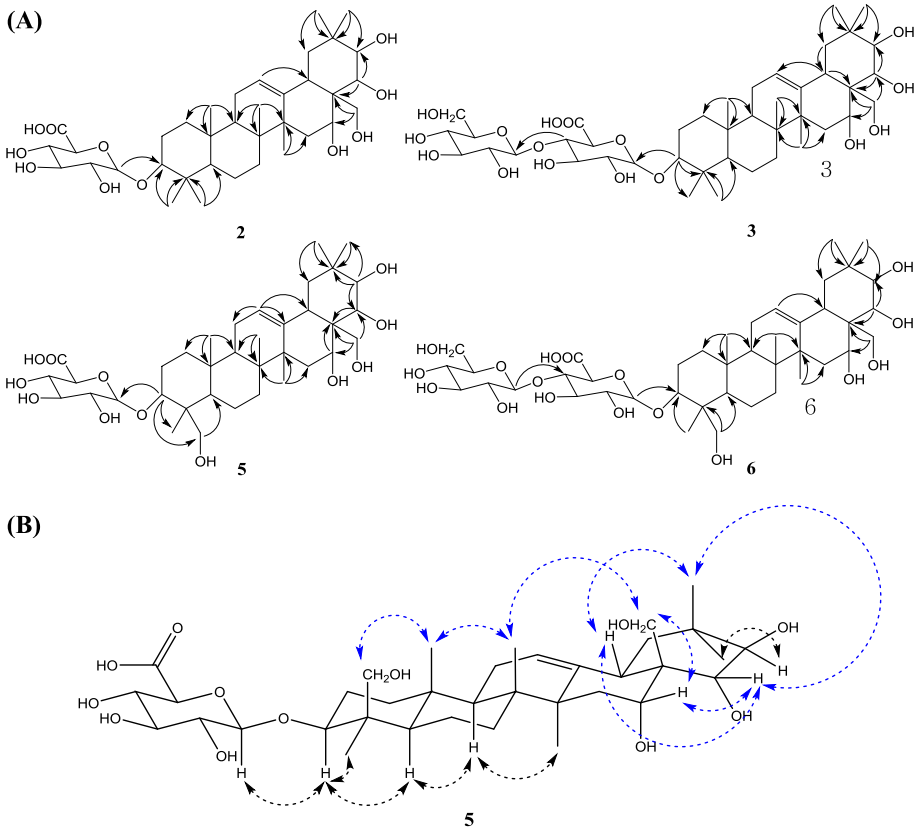

Fig 2. (A) Key HMBC correlations (^{1}H-^{13}C) for new compounds **2**, **3**, **5**, and **6**; (B) key ROESY correlations for compound **5**.

after the two-step reaction except for the deacylation and the cleavage of the glucose linkage. Therefore, the structure of **5** was identified as (3*β*,16*α*,21*β*,22*α*)-16,21,22,24,28-pentahydroxy-olean-12-en-3-*O*-*β*-D-glucopyranosiduronic acid.[23]

Compound **6** was isolated as a brown amorphous powder, with the molecular formula $C_{42}H_{68}O_{17}$, by the HRESIMS at *m*/*z* 867.4345 $[M+Na]^+$ (calcd for $C_{42}H_{68}O_{17}Na^+$, 867.4349) and at *m*/*z* 843.4384 $[M-H]^-$ (calcd for $C_{42}H_{67}O_{17}^-$, 843.4384). Its IR spectrum displayed strong absorptions for hydroxyl (3405 cm^{-1}), olefinic bond (1604 cm^{-1}), and glycosidic linkage (1033 cm^{-1}). The ^{1}H and ^{13}C NMR data of **6** suggested the structure as an olean-12-ene triterpenoid glycopyranosyl glucopyranosiduronic acid, exhibiting signals for six tertiary methyl groups [δ_H 0.78 (CH_3-25), 0.88 (CH_3-26), 1.33 (CH_3-29), 1.39 (CH_3-30), 1.49 (CH_3-23), 1.89 (CH_3-27)], an olefinic proton at δ_H 5.39 (br s) with two olefinic carbon signals at δ_C 123.3 (C-12) and 144.3 (C-13), one *β*-D-glucopyranosiduronic acid moiety [an anomeric proton at δ_H 5.09 (H-1′), along with five carbon signals at δ_C 106.2 (C-1′), 83.9 (C-4′), 76.9 (C-3′), 76.9 (C-5″), and 75.2 (C-2′)], and one *β*-D-glycopyranosyl moiety [one anomeric proton at δ_H 5.22 (H-1″), along with six carbon signals at δ_C 105.3 (C-1″), 78.8 (C-5″), 78.4 (C-3″), 75.4 (C-2″) and 72.0 (C-4″), 62.9 (C-6″)]. The ^{13}C NMR spectral peaks for compound **6** were very close to those for **3**. In particular, the signals for the carbons of the glycopyranosyl and glucopyranosiduronic acid moieties of **6** were fully in agreement with those of **3**, indicating the presence of *β*-D-glycopyranosyl-(1→4)]-*β*-D-glucopyranosiduronic acid. The linkage position was further confirmed in the HMBC experiment, showing the correlation from H-1′ (δ_H 5.09) to C-3 (δ_C 89.3) and from H-1″ (δ_H 5.22) to C-4′ (δ_C 83.9) of the *β*-D-glucopyranosiduronic acid (Fig. 2A). Thus, compound **6** was concluded to be (3*β*,16*α*,21*β*,22*α*)-16,21,22,24,28-pentahydroxyolean-12-en-3-yl-*O*-[*β*-D-glycopyranosyl-(1→4)]-*β*-D-glucopyranosiduronic acid.[23]

By analysing the ROESY data of compound **5**, we also confirmed that the overall skeleton and relative configurations of new compounds **2**, **3**, **5**, and **6** were identical with the escin series, after a two-step hydrolysis. Six known compounds **1**, **4**, and **7**–**10** were determined as protoaescigenin (**1**),[24] escinidin (**4**),[25] aesculuside B (**7**), escin Ia (**8**), escin Ib (**9**),[13] and isoescin Ia (**10**)[26] by comparison with literature data.

The cytotoxicity assay[27] was done at a concentration of 10 μg/mL to compare the cytotoxic effects of the total extract and partitioned fractions before and after a two-step hydrolysis (Fig. 3A). The *n*-BuOH fraction, containing a large amount of escins, showed strong cytotoxicity compared to fractions obtained after the two-step hydrolysis. Interestingly, compounds **1**–**7** isolated from the fraction with the two-step hydrolysis were evaluated to have much lower cytotoxic effects than compounds **8**–**10** from the *n*-BuOH part at concentration of 20 μM (Fig. S22). Additionally, dose-dependent cytotoxic effects of compounds **8**–**10** were ascertained at concentrations of 2, 5 and 10 μM (Fig. S23).

The *n*-BuOH and the other fractions from a two-step hydrolysis were evaluated for their PEDV inhibitory activities with 6-azauridine as positive control at 1, 2, 5, and 10 μg/mL (Fig. 3B).[28] Up to 2 μg/mL, both fractions showed similar and mild inhibitory effects on PEDV replication, proving the original horse chestnut's antiviral activities. The fraction after a two-step hydrolysis inhibited PEDV replication in a dose-dependent manner without cytotoxicity. The *n*-BuOH fractions above 5 μg/mL, which are expected to contain many escins, exhibited poor cell viability because of strong cytotoxic effects, even if it could show better PEDV inhibitory effects than the fraction from a two-step hydrolysis. Based on these data, the ten purified oleanane triterpenoids (**1**–**10**) were evaluated for their PEDV inhibitory effects with the same methods (Fig. S24). As compounds **8**–**10** showed

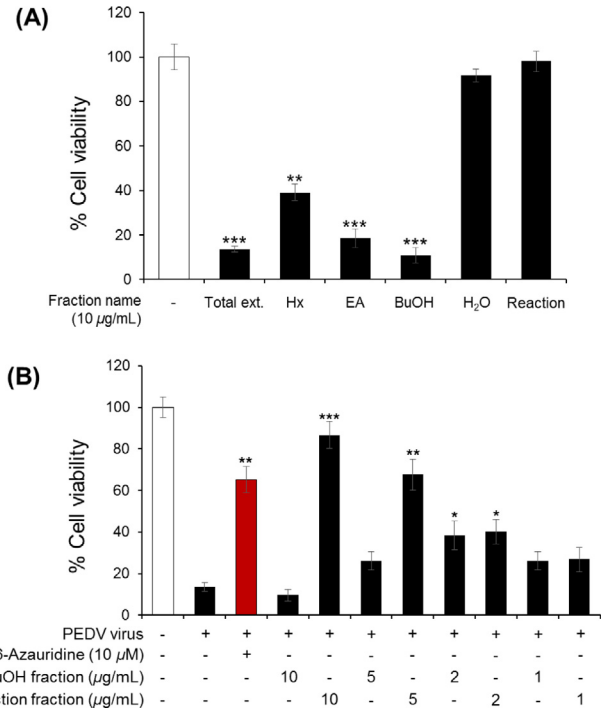

Fig. 3. (A) Cytotoxicity assay of fractions at 10 μg/mL. The reaction fraction had no cytotoxicity at 10 μg/mL and the *n*-BuOH fraction showed significant cytotoxicity. (B) CPE inhibition assay of the *n*-BuOH fraction and the reaction fraction at concentrations of 1, 2, 5, and 10 μg/mL. Up to 2 μg/mL, the *n*-BuOH fraction and the reaction fraction from a two-step hydrolysis showed similar activities, but at high concentrations, the *n*-BuOH fraction showed cytotoxic effects and the reaction fraction had PEDV inhibitory effects in dose-dependent manner.

strong cytotoxic effects on Vero cells at 20 μM, their PEDV inhibitory activities were evaluated at a concentration of 2 μM. Compounds **1**–**7** were tested at a concentration of 20 μM to compare their inhibitory effects on PEDV replication, providing less cytotoxicity in relatively high concentrations. Compound **4** showed the strongest inhibitory activity among the ten compounds **1**–**10**. Additionally, Compounds **4**–**6** exhibited concentration-dependent inhibition of PEDV replication at concentrations of 10, 20 and 40 μM, indicating improved cell viability from the two-step hydrolysis (Fig. S25). Based on cytotoxicity and CPE assays, structure-activity relationships (SARs) were studied. Isolated compounds **1**–**10** after the two-step hydrolysis suggested the presence of three important groups: (1) acylation at C-21, C-22 or C-28 (**1**–**7** and **8**–**10**), (2) methylation at C-24 (**1**–**3** and **4**–**6**), (3) existence of glycosidic linkages [(**1**–**3**) and (**4** and **5**–**7**)]. Group 1 (**1**–**7** and **8**–**10**) indicated that deacylation at C-21 could improve the cell viability (Figs.3A and S22). The PEDV inhibitory effects of group 2 (**1**–**3** and **4**–**6**) demonstrated that methylation at C-24 could reduce antiviral activity. Group 3 [(**1**–**3**) and (**4** and **5**–**7**)] showed that the absence of glycosidic linkage also improved the antiviral effects (Fig. S24).

During the PEDV replication, two key structural proteins, spike and nucleocapsid proteins, take part in important roles.[29] The spike protein regulates the entry stage of the virus[30] and binding of nucleocapsid protein to viral RNA is crucial for viral transcription.[31] Following the data of the cytotoxicity and CPE assays (Figs. S22–24), the five compounds **1** and **4**–**7** were selected for further evaluation. The inhibitory effects of compounds **1** and **4**–**7** on nucleocapsid protein synthesis at 20 μM were measured using Western blot (Fig. 4A).[32] The five compounds showed moderate inhibitory effects on nucleocapsid protein synthesis, and compound **4** significantly inhibited nucleocapsid protein synthesis. Thus, compound **4** was further analyzed for its effects in nucleocapsid and spike protein synthesis with Western blot at concentrations of 10, 20 and 40 μM, and it was found to inhibit PEDV replication in a concentration-dependent manner (Fig. 4B).

On the basis of the above findings, compounds **4** and **6** were also measured with key genes and proteins crucial for PEDV replication by real time qPCR (qPCR).[33] To measure the expression level of viral RNA encoding nucleocapsid and spike proteins, compounds **4** and **6** were treated in Vero cells at a concentration of 40 μM and total RNA was extracted for reverse transcription followed by polymerase chain reaction using the primers for PEDV (S-Table 1). Fig. 5A shows the RNA expression levels of two kinds of proteins with compounds **4**, **6** and positive control. When the inhibitory effect of compound **4** was analyzed in detail at the concentrations

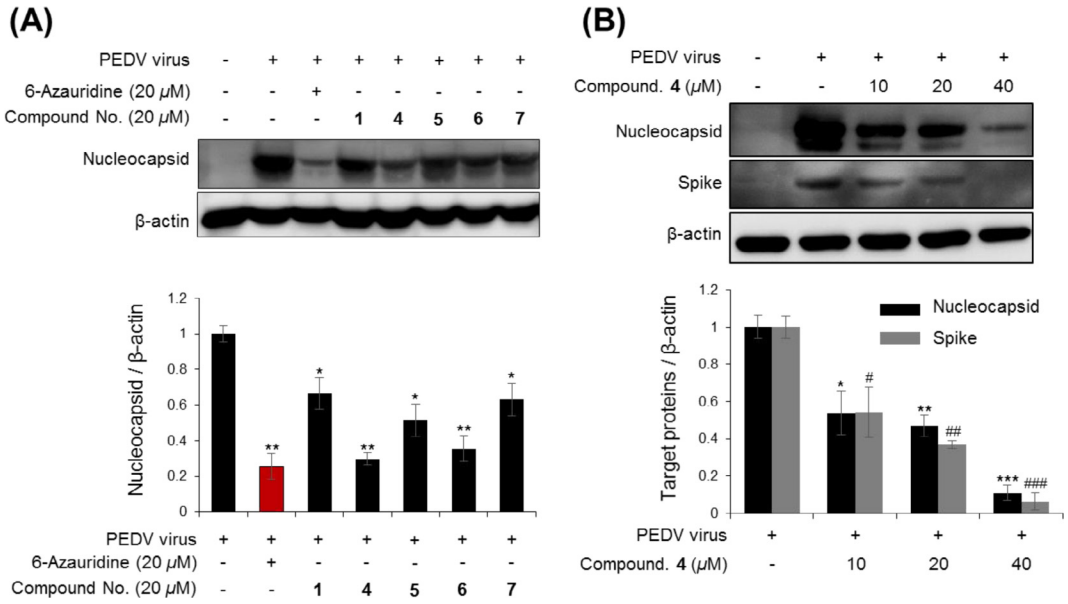

Fig. 4. (A) Inhibitory effects of compounds **1** and **4**–**7** on PEDV nucleocapsid synthesis, using Western blot assay. Compounds **1** and **4**–**7** inhibited PEDV nucleocapsid synthesis at a concentration of 2 μM. (B) Inhibitory effects of compound **4** on PEDV nucleocapsid and spike protein synthesis, using Western blot analysis.

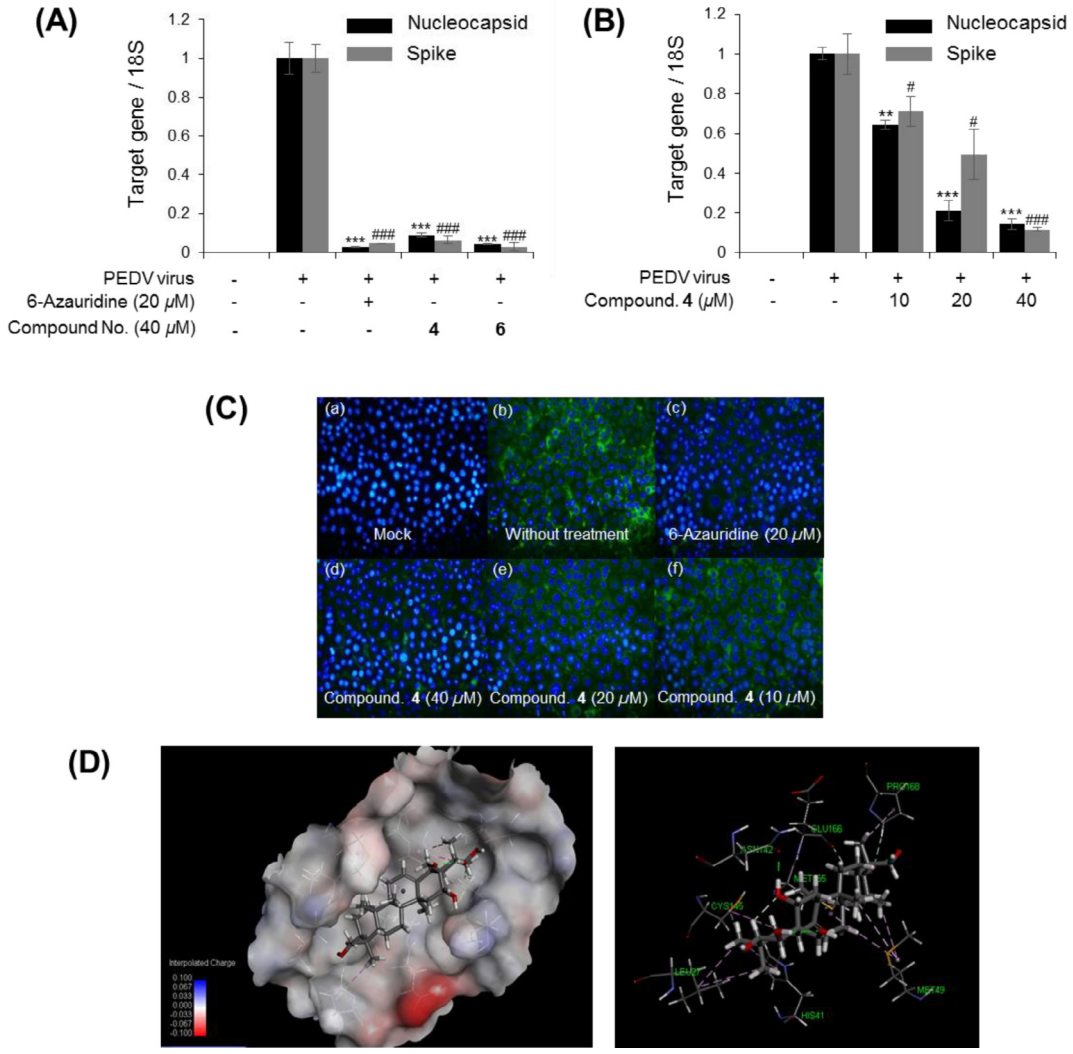

Fig. 5. (A) By RT-PCR analysis, inhibitory effects of compounds **4** and **6** on PEDV RNA expression encoding nucleocapsid and spike protein were evaluated. At a concentration of 40 μM, the two compounds showed significant biological effects. (B) By RT-PCR analysis, compound **4** was analyzed for its inhibitory effects on PEDV RNA expression encoding nucleocapsid and spike protein at the concentrations of 10, 20 and 40 μM. Compound **4** showed inhibitory effects on RNA expression in a concentration-dependent manner. (C) Immunofluorescence assay showed that PEDV replication on Vero cells was inhibited by compound **4** in a dose-dependent manner. (D) Docking simulation of 3CL protease (PDB: 3V3M) with compound **4** and its interaction.

of 10, 20 and 40 μM, compound **4** inhibited the RNA expression of nucleocapsid and spike proteins in a dose-dependent manner (Fig. 5B). On the basis of inhibition of PEDV RNA expression, compound **4** was further studied for its inhibitory effects on PEDV replication, by performing an immunocytochemistry assay (Fig. 5C).[34] We observed green fluorescence in virus-infected cells but no signals in mock-treated cells. This result revealed that compound **4** had noticeable inhibitory effects on PEDV replication in a dose-dependent manner at concentrations of 10, 20 and 40 μM.

3C-Chymotrypsin-Like protease (3CL protease) is vital for proteolytic processing of viral replication in coronaviruses. As escin was reported as a SARS-CoV 3CL protease inhibitor,[15] we performed docking modelling of compound **4** into the active site of SARS-CoV $3CL^{pro}$ (PDB ID code 3V3M).[35] The binding site was predicted by the 2D program of DS 4.0. As shown in Fig. 5D, the hydroxyl group of C22 and C16 of **4** formed hydrogen bonds with the oxygen atom of the carbonyl group of Glu166. Additionally, the methyl group of C23 and the B ring of **4** showed hydrophobic interactions with Cys145 and Leu27 through their side chains. The CDOCKER interaction energy was calculated to be −38.63 kcal/mol. The $3CL^{pro}$ binding energy value of compound **4** was unstable and weaker than that of the reference ligand 0EM. However, clear key amino acid interactions of compound **4** with $3CL^{pro}$, proposed the mode of action as inhibition of 3CL protease and explained inhibitory possibility of the SARS-CoV of escin derivatives.

This research demonstrated that including the four new compounds (**2**, **3**, **5**, and **6**), ten oleanane-type triterpenoids (**1**–**10**) were isolated from the seeds of *Aesculus turbinata* (Japanese horse chestnut). The cytotoxicity of the *n*-BuOH fraction was decreased with compounds **1**–**7** isolated from two-step hydrolysis. Especially, two compounds **4** and **6** showed strong inhibitory activities against PEDV in a dose-dependent manner. The present study proposed a way to utilize Japanese horse chestnut for treating PEDV with lowered cytotoxic effects and to increase the diversity of bioactive compounds.

Acknowledgements

This work was supported in part by grants from the Marine Biotechnology Program of the Ministry of Oceans and Fisheries (PJT200669) and the Korea Bioactive Natural Material Bank

(NRF-2012M3A9B8021570) of the National Research Foundation of Korea (NRF), which is funded by the Korean government.

Supplementary data

Supplementary data associated with this article can be found, in the online version, at http://dx.doi.org/10.1016/j.bmcl.2017.05.022.

References

1. van Boheemen S, de Graaf M, Lauber C, et al. *MBio*. 2012;3:e00473–12.
2. Graham RL, Donaldson EF, Baric RS. *Nat Rev Microbiol*. 2013;11:836–848.
3. Zaki AM, van Boheemen S, Bestebroer TM, Osterhaus AD, Fouchier RA. *N Engl J Med*. 2012;367:1814–1820.
4. de Wit E, van Doremalen N, Falzarano D, Munster VJ. *Nat Rev Microbiol*. 2016;14:523–534.
5. Wong G, Liu W, Liu Y, Zhou B, Bi Y, Gao GF. *Cell Host Microbe*. 2015;18:398–401.
6. Masters PS. *Adv Virus Res*. 2006;66:193–292.
7. Li C, Li Z, Zou Y, et al. *PLoS ONE*. 2013;8:e69997.
8. Zhang Z, Li S, Lian X. *Pharm Crop*. 2010;1:24–51.
9. (a) Yang XW, Zhao J, Hattori M. *J Asian Nat Prod Res*. 2008;10:259–265; (b) Yang XW, Zhao J, Cui YX, et al. *J Nat Prod*. 1999;62:1510–1513.
10. Hu JN, Zhu XM, Han LK, et al. *Chem Pharm Bull*. 2008;56:12–16.
11. Piao S, Kang M, Lee YJ, et al. *Urology*. 2014;84. 982.e1–7.
12. Sato I, Kofujita H, Suzuki T, Kobayashi H, Tsuda S. *J Vet Med Sci*. 2006;68:487–489.
13. Yoshikawa M, Murakami T, Matsuda H, Yamahara J, Murakami N, Kitagawa I. *Chem Pharm Bull*. 1996;44:1454–1464.
14. Wang P, Ownby S, Zhang Z, Yuan W, Li S. *Bioorg Med Chem Lett*. 2010;20:2790–2796.
15. Wu CY, Jan JT, Ma SH, et al. *Proc Natl Acad Sci*. 2004;101:10012–10017.
16. Chan PK. *Biochem Pharmacol*. 2007;73:341–350.
17. Chan PK, Zhao M, Che CT, Mak E. *J Nat Prod*. 2008;71:1247–1250.
18. Mojzisova G, Mojzis J, Pilatova M, et al. *Phytother Res*. 2013;27:159–165.
19. Podolak I, Galanty A, Sobolewska D. *Phytochem Rev*. 2010;9:425–474.
20. Rimmon A, Vexler A, Berkovich L, Earon G, Ron I, Lev-Ari S. *Biochem Res Int*. 2013;251752.
21. Sun H, Fang W, Wang W, Hu C. *Botanical Studies*. 2006;47:339–368.
22. The seeds of *A. turbinata* were collected from Seoul in 2014 and authenticated by Prof. W.K. Oh. A voucher specimen (SNU2014-006) was deposited in the herbarium of the College of Pharmacy, Seoul National University, Korea. The dried seeds of *A. turbinata* (1 kg) were extracted by sonication with 70% EtOH. The extract (195.1 g) was partitioned successively with *n*-hexane, EtOAc and *n*-BuOH. Since the *n*-BuOH-soluble fraction (70.8 g) contains a large amount of mixed triterpenoidal saponins called escins, this fraction was directly applied to hydrolysis reactions of two steps. Acyl group hydrolysis was done at 90 °C with 0.5 N NaOH in 50% EtOH aqueous solution for 2 h. Further partial hydrolysis of the glucose moieties was also followed with 1.0 N HCl in 50% EtOH aqueous solution at 90 °C for 2 h. This reaction mixture was directly placed on an HP-20 CC (10 × 60 cm) to discard salt, washed with 10% EtOH (3 L), and finally eluted with EtOH (3 L) for the saponin fraction. The partial saponin fraction (5.59 g) was then chromatographed over an RP-C_{18} CC (40–63 μm particle size) and eluted with a gradient solvent system of MeOH:H_2O (from 4:6 to 1:0), to yield five fractions (F1–F5). Fraction F1 was further applied to semi-preparative HPLC [RS Tech Optima Pak C18 column (250 × 10 mm, particle size 5 μm)]; (0–5 min: A:B (75:25), 5–24 min: A:B (75:25–40:60), 24–34 min: B; 0.1% formic acid in H_2O (A) and MeCN (B); flow rate 2 ml/min; UV detection at 205 and 254 nm) to isolate compounds **6** and **7**, respectively. Fraction F2 was also chromatographed by preparative HPLC (0–5 min; A:B (75:25), 5–25 min; A:B (75:25– 60:40), 25–35 min; B) to provide compounds **2**, **3** and **5**. Purification of fraction F4 by preparative HPLC (mobile phase MeCN/H_2O (30:70–60:40) over 25 min) resulted in the isolation of compound **4**. Fraction F5 was purified by preparative HPLC (mobile phase MeCN/H_2O (30:70–60:40) over 25 min) to provide compound **1**. Compounds **8**–**10** were isolated from the *n*-BuOH fraction of the dried seeds of *A. turbinata* extract by semi-preparative HPLC using an isocratic solvent of 40% MeCN with 0.1% formic acid over 40 min.
23. β,16α,21β,22α)-16,21,22,28-tetrahydroxyolean-12-en-3-O-β-D-glucopyranosiduronic acid (**2**): amorphous powder; $[\alpha]_D^{25}$ +19.8 (c 0.1, MeOH); IR (KBr) νmax 3375, 2947, 2834, 1658, 1451, 1411, 1117, 1023 cm^{-1}; see Table 1 for ^1H (500 MHz) and ^{13}C NMR (125 MHz); HRESIMS *m/z* 665.3906 (calcd for $C_{36}H_{57}O_{11}$ $[M-H]^-$, 665.3906). *(3β,16α,21β,22α)-16,21,22,28-tetrahydroxyolean-12-en-3-yl-O-[β-D-glycopyranosyl-(1→4)]-β-D-glucopyranosiduronic acid* (**3**): amorphous powder; $[\alpha]_D^{25}$ +12.5 (c 0.1, MeOH); IR (KBr) ν_{max} 3390, 2952, 2834, 1658, 1456, 1412, 1028 cm^{-1}; see Table 1 for ^1H (500 MHz) and ^{13}C NMR (125 MHz); HRESIMS *m/z* 827.4434 (calcd for $C_{42}H_{67}O_{16}$ $[M-H]^-$, 827.4435). *(3β,16α,21β,22α)-16,21,22,24,28-pentahydroxyolean-12-en-3-O-β-D-glucopyranosiduronic acid* (**5**): amorphous powder; $[\alpha]_D^{25}$ +32.7 (c 0.1, MeOH); IR (KBr) ν_{max} 3385, 2952, 2834, 1657, 1456, 1412, 1028 cm^{-1}; see Table 1 for ^1H (800 MHz) and ^{13}C NMR (200 MHz); HRESIMS *m/z* 681.3852 (calcd for $C_{36}H_{57}O_{12}$ $[M-H]^-$, 681.3856). *(3β,16α,21β,22α)-16,21,22,24,28-pentahydroxyolean-12-en-3-yl-O-[β-D-glycopyranosyl-(1→4)]-β-D-glucopyranosiduronic acid* (**6**): amorphous powder; $[\alpha]_D^{25}$ +10.9 (c 0.1, MeOH); IR (KBr) vmax 3405, 2942, 1604, 1051, 1033 cm^{-1}; see Table 1 for ^1H (800 MHz) and ^{13}C NMR (200 MHz); HRESIMS *m/z* 843.4384 (calcd for $C_{42}H_{67}O_{17}$ $[M-H]^-$, 843.4384).
24. Konoshima T, Lee KH. *J Nat Prod*. 1986;49:650–656.
25. Chen YJ, Takeda T, Ogihara Y, Iitaka Y. *Chem Pharm Bull*. 1984;33:3378–3383.
26. Yoshikawa M, Murakami T, Yamahara J, Matsuda H. *Chem Pharm Bull*. 1998;46:1764–1769.
27. Vero cells (African green monkey kidney cell line; ATCC CCR-81) were obtained from American Type Culture Collection (ATCC, Manassas, VA, USA). Cells were grown in Dulbecco's Modified Eagle's Medium (DMEM) supplemented with 100 U/mL penicillin, 100 μg/mL streptomycin and 10% fetal bovine serum (FBS). PEDV was provided by Choong Ang Vaccine Laboratory, Korea. Virus stock was maintained at −80 °C before use. To assess the cell viability, a MTT (3-(4,5-dimethyl-2-thiazolyl)-2,5-diphenyl-2*H*-tetrazolium bromide) assay was carried out. Vero cells were seeded for 24 h in 96-well plates at 1×10^5 cells per well. Then, the cells were exposed to different concentrations of fractions and compounds for 48 h. The final concentration of DMSO was maintained at 0.05% (v/v) to avoid solvent toxicity. Twenty microliters of MTT solution (2 mg/mL) was then added to cultures and incubated for 4 h. Formazan crystals were dissolved with 100 μL of DMSO, and the optimal densities (OD) were measured at 550 nm.
28. Vero cells were grown in 96-well plates at 1×10^5 cells per well. After 24 h, the medium was removed and washed with phosphate buffered saline (PBS). PEDV (0.01 MOI) were inoculated onto confluent monolayers of Vero cells for 2 h. The media were replaced by DMEM with different concentrations of compounds. After 72 h of incubation at 37 °C in a 5% CO_2-balanced air incubator, cells were replaced with DMEM. Then, 20 μL of MTT solution (2 mg/mL) was added to each well and incubated for 4 h.
29. Song D, Park B. *Virus Genes*. 2012;44:167–175.
30. Cruz DJ, Kim CJ, Shin HJ. *Virus Res*. 2008;132:192–196.
31. Baric RS, Nelson GW, Fleming JO, et al. *J Virol*. 1988;62:4280–4287.
32. Whole-cell lysates were prepared by scraping adherent-cultured cells with 100 μL of lysis buffer (0.5% NP-40, 50 mM NaF, 1 mM EDTA, 120 mM NaCl, and 50 mM Tris-HCl (pH 7.6)) and centrifuged at 12,000 rpm for 20 min. Protein concentrations of the supernatant were calculated using a protein assay kit (Bio-Rad Laboratories, Hercules, CA, USA). Aliquots of lysates were separated by 10–12% SDS-PAGE and electrophoretically transferred to PVDF membranes (PVDF 0.45 μm. Immobilon-P, USA). Membranes were incubated overnight with antibodies against spike (S) protein, nucleocapsid (N) (AbFrontier Co., Ltd., Seoul, Korea) or mouse monoclonal actin, and further incubated with secondary antibodies. Protein bands were detected using an enhanced chemiluminescence Western blotting detection kit (Thermo Scientific).
33. Quantitative real-time PCR was performed using the StepOnePlus Real-Time PCR System (Applied Biosystems, Foster City, CA, USA). Vero cells were seeded at 90% confluence in 6-well plates, infected with PEDV (0.01 MOI), and incubated for 2 h. Then, the medium was replaced by DMEM and cultured with different concentrations of compounds. After 24 h, total RNA from the cells was isolated by the TRIzol method and reverse transcribed using random primer (iNtRON Biotechnology, Seongman, Korea) according to the manufacturer' protocol. Amplifications were carried out using selective primers for PEDV, which are listed in S-Table 1 (Supporting Information), using 2 μL of cDNA and Maxima SYBR Green qPCR master mix 2X (Thermo Scientific, Rockford, IL, USA). Cyclic conditions were as follows: initial denaturation at 95 °C for 10 min, 40 cycles with 95 °C for 15 s and 60 °C for 1 min.
34. Cells were grown on sterilized glasses slides, and PEDV (0.01 MOI) was inoculated to the cell monolayers for 2 h. The solution was replaced with DMEM, treated with compounds for 24 h, washed in PBS (pH 7.4) and fixed with a 4% paraformaldehyde solution for 30 min at room temperature. The slides were blocked with 1% BSA for 1 h, and incubated with monoclonal antibody against N protein of PEDV (AbFrontier Co., Ltd., Seoul, Korea) diluted 1:50 with PBS (pH 7.4) for 24 h. The slides were washed with PBS, and incubated with FITC-conjugated goat anti-RbIgG antibody (Abcam, Cambridge, UK) for 1 h. After washing three times with PBS (pH 7.4), the slides were stained with 500 nM DAPI solution for 10 min at room temperature and washed with PBS (pH 8.0) three times. Mounting reagent (Vectashield, Vector Laboratories Inc., Burlingame, CA, USA) was used. The slides were examined under a fluorescence microscope (Olympus ix70 Fluorescence Microscope, Olympus Corporation, Tokyo, Japan).
35. Jacobs J, Grum-Tokars V, Zhou Y, et al. *J Med Chem*. 2013;56:534–546.